FE25886

NTIS®
Information is our business.

H-COAL FLUID DYNAMICS TOPICAL REPORT. PART I. LITERATURE SEARCH

COPY

AMOCO OIL CO., NAPERVILLE, IL. RESEARCH AND DEVELOPMENT DEPT

MAY 1978

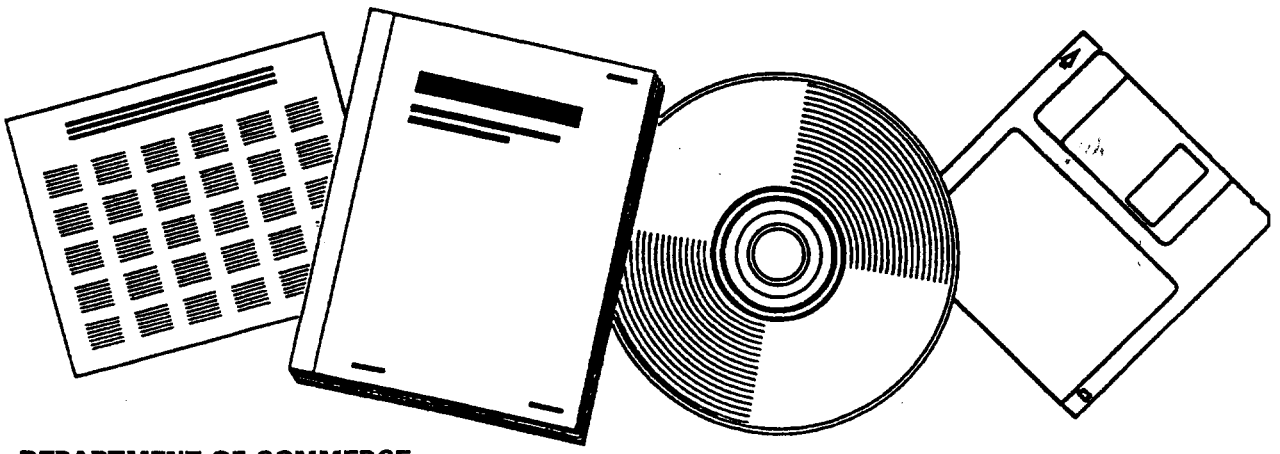

U.S. DEPARTMENT OF COMMERCE
National Technical Information Service

FE-2588-6
Distribution Category UC-90d

H-COAL FLUID DYNAMICS

TOPICAL REPORT

PART I
LITERATURE SEARCH

I. A. Vasalos
E. M. Bild
D. F. Tatterson
C. C. Wallin

Date Published: May, 1978
Amoco Oil Report No. M78-39
Date: May 3, 1978

PREPARED FOR THE UNITED STATES
DEPARTMENT OF ENERGY
UNDER CONTRACT NO. EF-77-C-01-2588

Amoco Oil Company
P. O. Box 400
Naperville, Illinois
60540

TABLE OF CONTENTS

Preceding page blank

TABLE OF CONTENTS

ABSTRACT

An analysis of literature related to the fluid dynamics of gas/liquid/solid systems has provided information useful in understanding the fluid dynamics of the H-Coal reactor. In the H-Coal process, the catalytic hydroliquefaction of coal takes place in an ebullated bed reactor, where catalyst pellets, coal and fly ash fines, liquids, and gas are present. The need to understand the hydrodynamic properties of the H-Coal reactor necessitated a literature search in the following areas:

1) The hydrodynamics of fluidization
2) Experimental techniques in multi-phase flow.
3) Physical properties of coal/oil mixtures.

The section on hydrodynamics of fluidization reviews prior work on liquid/solid fluidization, gas/liquid vertical flow, and gas/liquid/solid fluidization. Experimental conditions, data correlations, and models in these areas are reviewed. Bubble behavior in liquids and liquid fluidized beds is also covered. The bulk of existing data is for fluidization with air and water in small-scale equipment.

This report also reviews experimental techniques available for studying multi-phase systems. Techniques using external detectors such as gamma-ray scans, radioactive tracers, and some sonic probes are favored for use in the H-Coal project because they do not disturb the flow. Light, impedance, and conductivity probes which require detectors inside the reactor are also reviewed.

The physical properties of coal/oil slurries and papers on viscosity measurement of these slurries are also discussed. The literature indicates that the viscosity of these slurries is a function of temperature, solids volume fraction, and solids particle size distribution. Empirical correlations for analyzing the viscosity data are also reviewed.

INTRODUCTION

Background

The H-Coal process, developed by Hydrocarbon Research, Incorporated (HRI), involves the direct catalytic hydroliquefaction of coal to low-sulfur boiler fuel or synthetic crude oil. The process has been demonstrated by HRI in their Process Development Unit (PDU) at Trenton, New Jersey. This unit is capable of processing up to three tons of dried coal per day. A 200-600 ton/day pilot plant is under construction at Catlettsburg, Kentucky. This plant will be operated by Ashland Synthetic Fuels, Incorporated.

In the H-Coal process, coal is dried, pulverized to approximately 100-mesh size, and slurried with coal-derived oil. This slurry is charged with hydrogen to an ebullated bed reactor containing a hydrogenation catalyst. The reactor operates between 800-900°F and 2000-3200 psi.

The unique feature of HRI's H-Coal process is the use of an ebullated bed as the means of achieving good mixing between the catalyst particles, the slurried coal, and the hydrogen gas. The catalyst is in extruded form and is similar to those used in petroleum hydrotreating processes. Typically, catalyst dimensions are 1/16" diameter and 3/16" length.

A schematic diagram of the reactor used in the Process Development Unit is shown in Figure 1. A key feature of the H-Coal reactor is a large capacity internal circulation pump (ebullating pump) which takes suction from a point in the reactor near the top of the fluidized bed. The discharge from the ebullating pump is mixed with the fresh feed slurry and make-up gas and recycled to the reactor through a specially designed distributor. The ratio of the ebullating flow to fresh feed flow may be as high as 10:1.

In the ebullating bed the upward flow of the slurried coal and gases forces the catalyst bed to expand. The expansion of the bed allows fine particles such as coal and ash to pass through the bed and out with the liquid stream, leaving the catalyst within the bed.

Downstream of the Process Development Unit (PDU) reactor, the product slurry is separated into various streams as shown in Figure 2. The product pressure is let down at about reactor temperature to atmospheric pressure in a flash drum. During the flash, a portion of the hydrocarbon liquids is flash-vaporized and fed to the atmospheric distillation tower. The bottoms from the flash drum are directed either to a hydroclone or to a vacuum distillation tower. The feed slurry oil used to disperse the coal particles may come from the atmospheric tower bottoms, the hydroclone overflow, or the vacuum distillation overhead. The weight ratio of slurry oil to solids in the feed is typically about 1.5-2.0. The composition of the recycled slurry oil varies depending on the mode of operation (fuel oil versus synthetic crude), catalyst age, and the properties of the processed coal.

The variation in feed composition and slurry concentration causes significant variation in the feed viscosity. These viscosity changes affect bed expansion and lead to a range of operating conditions, as shown below (204):

% Expansion of Catalyst Bed	63-80
Reactor Slurry Composition:	
% Resid	13-18
% Solids (Coal and Ash)	9-22
Slurry Properties (at Reactor Conditions):	
Viscosity, CP	0.2-0.5
Specific Gravity, gr/cc	0.6-0.7
Gas Velocity, Ft/Sec	0.04-0.16
Slurry Velocity, Ft/Sec	0.07-0.18

Scope of the Amoco Work

Although the HRI work has made significant contributions in understanding the fluid dynamics of three-phase fluidized systems, most of this work was carried out with clear liquids where fines were not present. The need to extend the HRI work to the H-Coal system led to a two-year contract with the objective of studying the hydrodynamics of the H-Coal reactor. Application of this work would improve the control of the ebullating bed in the H-Coal reactor. The project is divided into three parts:

Part I:	Review of Prior Work
Part II:	Construction of a Cold Flow Model and Data Collection
Part III:	Mathematical Model

The review of prior work will consist of a literature search of gas/liquid/solid systems as related to the H-Coal process. The results of the literature search will serve as a basis for data collection and model development.

Data will be collected in a cold flow apparatus consisting of a transparent reactor and auxiliary equipment to handle the ebullated catalyst and circulating slurries and gases. The unit will be equipped with experimental techniques to measure pressure drop across the catalyst bed, average gas residence time, gas residence time as a function of height above the distributor, and liquid mixing. Liquids selected for operation of the unit will have the same physical properties at room temperature which the H-Coal liquids have under reactor conditions.

The data generated in the cold flow unit will be used to develop a mathematical model defining the following: a) steady-state ebullated bed conditions as a function of operating parameters; b) criteria for bed stability. In addition to the data collected under this project, the model will also be based on information currently available in the literature.

The objective of this report is to present the results of the review of prior work. Three areas will be reviewed:

1) The hydrodynamics of fluidization.
2) Experimental techniques for multi-phase systems.
3) Physical properties of coal/oil mixtures.

The open literature and the prior work of HRI have been reviewed in the above areas. The list of references cited, sources searched, and methods of searching for this report are described in the appendix. In many cases more papers were found in a given area than was practical to discuss in the text. These papers are also contained in the list of references.

REVIEW OF THE HYDRODYNAMICS OF FLUIDIZATION

The objective of this section is to review the available data, correlations, and models of three-phase systems. This area has been subdivided into the following areas to be considered:

1) Liquid/solid fluidization.
2) Vertical gas/liquid flow.
3) Gas/liquid/solid fluidization.

The review of these areas will serve as a basis for the development of a mathematical model to correlate three-phase fluidization data. According to Darton and Harrison (70), the model should fulfill the following criteria:

1) The model should reduce to a suitable liquid/solid fluidization model as the volume fraction of gas approaches zero.
2) The model should reduce to a suitable gas/liquid model as the volume fraction of solids approaches zero.
3) The sum of the volume fraction of the various phases should add up to one.
4) The model should predict whether the bed will expand or contract upon the addition of gas.

These criteria stress the importance of applying knowledge of liquid/solid and gas/liquid systems in developing an understanding of gas/liquid/solid fluidization.

Liquid/Solid Fluidization

Understanding the behavior of liquid/solid fluidized systems is one important phase of this work. Several reviews have been published in this area. In a recent article, Garside and Al-Dibouni (5) reviewed available liquid/solid fluidization data and related correlations. Fifteen correlations proposed in the literature were also listed in the same article. In another publication, Barnea and Mizrahi (1) present a literature review of this area.

In the following sections, several of the more prominent correlations for bed expansion in liquid/solid fluidized systems discussed in these two papers are reviewed. Special attention is given to correlations involving non-spherical particles.

Correlations.--The correlations reviewed in this section are summarized in Table I.

The most widely used method of correlating liquid/solid fluidization data is that of Richardson and Zaki (6). Their analysis recognizes the similarities between sedimentation and fluidization. They observed that the settling velocity of a suspension relative to a fixed horizontal plane was equal to the upward liquid superficial velocity needed to maintain the suspension at the same concentration.

As shown in Table I, the correlation relates the liquid volume fraction (ϵ_l) due to bed expansion to the ratio of the superficial liquid velocity (U_l) to the terminal velocity of a single particle (U_t):

$$\epsilon_l^n = U_l/U_t \tag{1}$$

For spherical particles:

$$n = f(Re_t, d/D) \tag{2}$$

where: $Re_t = d_p \rho_l U_t/\mu_l$, Reynolds number
d = particle diameter
ρ_l = liquid density
μ_l = liquid viscosity
D = bed diameter

The functional form of Equation 2 for different ranges of Reynolds number is given in Table I. It should be noted that for values of Re_t less than 0.2 or greater than 500, the exponent n in Equation 1 is independent of liquid viscosity.

For non-spherical particles, the exponent n in Equation 2 also becomes a function of particle shape. For turbulent Reynolds numbers (> 500), Richardson and Zaki found:

$$n = 2.7\, K^{0.16} \tag{3}$$

where: $K = (\pi/6) d_s^3/d_p^3$ (4)

The constant K is the particle shape factor proposed by Heywood (187). In Equation 4, d_s is the diameter of a sphere with the same volume as the particle, and d_p is the diameter of a circle of the same area as the projected particle when lying in its most stable position.

A modification to the Richardson-Zaki (R-Z) correlation to account for non-spherical particles has been proposed by Fouda and Capes (4). The equation is reported in Table I. In addition to the parameters used by the R-Z correlation, Fouda and Capes introduced a parameter (K') which corrects the solid volume fraction for the effective hydrodynamic volume of the particles.

Barnea and Mizrahi (1) developed a correlation based on a relationship between a modified drag coefficient (C_{DM}) and a modified particle Reynolds number. The liquid (ϵ_l) and solids (ϵ_s) holdups are indirectly included in this relationship. Their correlation is reported in Table I. Barnea and Mizrahi argue that for multi-particle systems the effective density and viscosity of the liquid phase changes due to the effect of the fluidized particles. The authors propose that the effect of suspended particles on the liquid viscosity is similar to that suggested by Mooney (193):

$$\frac{\mu_e}{\mu_l} = \exp\left(\frac{5/3\ \epsilon_s}{1 - \epsilon_s}\right) \tag{5}$$

where: μ_e = effective viscosity of fluidized bed
μ_l = viscosity of liquid
ϵ_s = solids volume holdup

The effect of particles on the density of the fluidized bed is given by:

$$\rho_b = \rho_s \epsilon_s + \rho_l (1 - \epsilon_s) \tag{6}$$

where: ρ_s = density of particles
ρ_l = density of liquids

In addition to the effect of solids on the bed viscosity and density, wall effects also become important in determining the particle terminal velocity. The wall effect is represented by the following relationship:

$$\frac{U_r}{U_t} = \frac{1}{1 + \epsilon_s^{1/3}} \tag{7}$$

where: U_r = relative velocity between the particles and the fluid in the bed.

With the modifications given by Equations 5 through 7, a correlation was then developed between the drag coefficient and the Reynolds number. This is shown in Table I.

Wallis (61) and Wen and Yu (10) have also proposed general correlations for sedimentation and particulate fluidization in terms of particle Reynolds number, drag coefficients, and solids fractions.

Wallis (9) has also presented a general correlation between particle size (r, radius), liquid volume fraction (ϵ_l), and flux of liquid relative to particles (j_l). An approximation of this correlation is shown in Table I.

Validation of Correlations with Existing Data.--In this section the application of the Richardson-Zaki correlation will be tested using liquid/solid fluidization data. No effort will be made at this time to test the other correlations reported in Table I.

Available data with particles having properties similar to those of coal conversion catalysts are shown in Table II. Of these data, only the data of HRI (202,203) and Blum, et al. (66), involving cylindrical particles, will be considered here. HRI's data were first analyzed to determine whether they correlate via the R-Z correlation. In Figures 3 and 4 the liquid holdup (ϵ_l) is plotted versus the superficial velocity (U_l). From these plots the particle terminal velocity (U_t) can be found by extrapolating to $\epsilon_l = 1$. The exponent n in Equation 1 can be found by plotting on log-log paper ϵ_l vs. U_l/U_t. This is done for HRI's data in Figures 5 and 6. The slope of the line in these figures is the exponent n. Figure 6 indicates that for the transformer oil and linseed oil, the exponent n is the same. This is because for this case the Reynolds number is very small and hence, as indicated in Table I, n becomes independent of Re_t (liquid viscosity). Table I suggests that the exponent n for cylinders might be a function of the terminal particle Reynolds number (Re_t) and the particle length (l) to diameter (d) ratio; thus, n is plotted as a function of Re_t in Figure 7. Equation 2 for a sphere is also shown in the figure. Figure 7 indicates that n has a strong dependence on the l/d ratio at constant Re_t. Extrapolation of the data for a given l/d to Re_t values exceeding 500 gives the values of the exponent n for the various l/d ratios. These results are shown in Figure 8 as a function of the Heywood factor K. Also shown in the figure is Equation 3.

Blum and Toman (66) have also measured the expansion of beds containing cylindrical particles. A summary of their experimental conditions is also shown in Table II. Throughout their experiments the particle Reynolds number (Re_t) was greater than 500. Values of n and K from their studies were determined in a manner similar to that used for HRI's data. These results are also included in Figure 8.

HRI's data in Figure 8 indicate a much stronger dependency of n on K than is suggested by Equation 3. The results of Blum and Toman at K = 0.55 agree reasonably well with those of Richardson and Zaki. However, at K = 0.77 the agreement is poor. The results in Figure 8 indicate that more experiments need to be performed with cylindrical particles of varying l/d ratios to determine the effects of particle shape on the Richardson-Zaki index, n. The particle Reynolds number in these experiments should be varied over the range covered in Figure 7.

Non-Newtonian Liquid/Solid Fluidization.--Brea, Edwards, and Wilkinson (2) studied the flow of titanium dioxide slurries through fixed and fluidized beds of uniform spherical particles. The viscosity of the slurries was measured by an in-line tubular viscometer. The wall shear stress for these slurries exhibited a power law dependency on the shear rate:

$$\tau_W = M' \left(\frac{8U_m}{D_c}\right)^{n'} \tag{8}$$

where: τ_W = wall shear stress
U_m = mean velocity in viscometer
D_c = diameter of capillary in viscometer
M' = rheological parameter

The authors develop a friction factor/Reynolds number relationship for the flow of non-Newtonian slurries through packed beds. They found that if the relationship is to be extended to fluidized beds, it must be modified to account for d/D effects. The modified relation leads the authors to suggest that for beds with minimum fluidization Reynolds numbers (Re_f) less than 40, n in Equation 1 also becomes a function of n'. For beds with Re_f greater than 40, n is independent of n'. For slurries with n' = 1 (Newtonian), the authors found good agreement between experimentally measured values of n and those predicted by Equation 2.

Yu, Wen, and Bailie (11) have also studied the flow of power law fluids through packed and fluidized beds. The beds consisted of glass balls, green peas, and nylon balls with diameters in the range of 0.08 to 0.35". The fluids were water solutions of polyox-205 and polyox-301 (Union Carbide Corporation). These authors also suggest that in the Stokes flow region ($Re_t < 2$), n in Equation 1 becomes a function of n' from Equation 8.

Vertical Gas/Liquid Systems

Darton and Harrison (70) have indicated that the second criterion for the development of a mathematical model of gas/liquid/solid fluidized systems is that such systems should behave like gas/liquid systems when the solids concentration tends to zero. Hence, it is imperative to understand the important aspects of vertical gas/liquid flow.

The literature indicates that for the range of superficial gas and liquid flow rates of interest to three-phase fluidized systems, there are two gas/liquid flow patterns: a) The ideal bubbly regime in which the bubbles rise as a uniform, steady cloud with little interaction; and b) The churn-turbulent regime which is a transition

region between ideal bubbly flow and fully developed slug flow. The churn-turbulent regime is dominated by bubble coalescence; hence the bubble size is larger than in the ideal bubbling regime, bubble wake effects become important, and the flow is unsteady.

In the following sections, bubble and slug behavior is reviewed. For convenience, this area has been divided into the following categories: bubble formation, rise velocity of single bubbles, bubble wakes, bubble coalescence, bubble breakup, swarms of bubbles, and slug behavior.

Bubble Formation.--Bubble formation at orifices is an area of extensive studies by many investigators. An excellent review of these studies is presented by Wallis (61). It has been found that in general the initial bubble size depends on the gas flow through the orifice. For small gas flows the correlations are based on a static force balance between surface tension and buoyancy forces. Katatcludze and Styrikovich (46) suggest that in this case the initial bubble radius (r) is related to the orifice radius (r_o) by the following equation:

$$r = \left[\frac{\sigma r_o}{g(\rho_l - \rho_g)}\right]^{1/3} \tag{10}$$

where: σ = surface tension, dynes/cm
ρ_l, ρ_g = liquid and gas densities in gm/cc

Koide, et al. (42,43) have extended this type of analysis to larger gas flow rates through porous and perforated plates. They found correlations of the following form:

$$r\left(\frac{g\rho_l}{\sigma r_o}\right)^{1/3} = f(We, Fr) \tag{11}$$

where: We = $\delta U_g^2 \delta \rho_l / \sigma$, Weber number
Fr = $U_g^2 / g\delta$, Froude number
δ = pore diameter of gas distributor, cm
$U_{g\delta}$ = gas velocity through pore, cm/sec

Davidson and Amick (25) have also studied the formation of bubbles at an orifice at larger gas flow rates in inviscid liquids. They proposed the following relationship which gives the volume of the bubble (v_b) as a function of the volumetric flow rate (Q_g) through the orifice:

$$v_b = 1.138 \frac{Q_g^{6/5}}{g^{3/5}} \tag{12}$$

Davidson and Schuler (26) have extended this work to viscous fluids with the following correlation:

$$v_b = \left(\frac{4r}{3}\right)^{1/3} \left(\frac{15\mu_1 Q_g}{2g(\rho_1-\rho_g)}\right)^{3/4} \quad (13)$$

Krishnamurthi, et al. (44,45) have also proposed correlations for bubble volumes formed in viscous fluids.

Rising Velocity of Single Bubbles.--Peebles and Garber (55) have correlated the terminal rising velocity of isolated gas bubbles (U_t) as a function of bubble radius (r_e) and gas and liquid properties. For the case when the gas density and viscosity are negligible compared to those of the liquid, four distinct regions of bubble velocity were noted.

The terminal velocity in each region is given in Table III. For a given gas/liquid combination, progression through Regions I to IV results from increasing bubble size.

If the bubble size becomes larger than that studied by Peebles and Garber, the bubble assumes a spherical cap shape. Davies and Taylor (27) have studied the rise of single spherical cap bubbles in inviscid fluids. They assumed that the flow around the nose of the bubble would be given by the potential flow solution for flow around a solid sphere. This assumption leads to:

$$U_b = 2/3\sqrt{gR} \quad (14)$$

where R is the radius of curvature for the bubble. They found that this expression was adequate for air bubbles rising in water and nitrobenzene. In terms of equivalent radius (r_e),which is the radius the bubble would have it it were a sphere, Equation 14 becomes:

$$U_b = 1.0\sqrt{gr_e} \quad (15)$$

This expression leads to a constant drag coefficient of 2.6 to 2.7 for spherical cap bubbles.

Grace (30) has presented an excellent review of the shapes and velocities of bubbles rising in infinite liquids. Data from eight sources, including Kojima, et al. (41) and Davenport, Richardson, and Bradshaw (28) were analyzed. For the case where gas density and viscosity are small compared to that of the liquid, bubble shape and velocity are functions of three dimensionless groups:

$$\text{Reynolds Number} = \rho_1 d_e U_t/\mu_1$$

$$\text{Eotvos Number} = gd^2_e(\rho_1-\rho_g)/\sigma$$

$$\text{Morton Number} = g\mu_1^4/\rho_1\sigma^3$$

A generalized plot of Reynolds number versus Eotvos number with the Morton number as a parameter is presented in Reference 90. Three distinct bubble shape regions were found: spherical, ellipsoidal, and spherical cap. In a later paper, Grace, Wairegi, and Nguyen (29) extend this plot to include drops. They also develop a correlation relating the height-to-width ratios of drops and bubbles to the Morton and Eotvos numbers.

Bubble Wakes.--As bubble size and velocity increase, bubble wake effects become important. The wake may influence trailing bubbles by increasing their velocity. Ultimately this interference may lead to bubble coalescence and thereby play a role in the transition from ideal bubbly flow to the churn-turbulent pattern.

Narayanan, et al. (51) have classified the wakes behind bubbles rising in liquids into five different classes. The class is a function of the bubble Reynolds number. For Reynolds numbers less than 2 (Class I), the bubbles are spherical in shape with a thin, trailing wake. Between a Reynolds number of 2 and 7 (Class II), the bubbles develop a cusp at the rear but still retain a thin, trailing wake. At Reynolds numbers between 7 and 80 (Class III), the bubbles become spherical cusps and develop stable wake vortices. Between a Reynolds number of 80 and 300 (Class IV), the spherical cap begins to oscillate, shedding its vortices. Above a bubble Reynolds number of 300 (Class V), the bubble becomes irregularly shaped and the wake becomes turbulent. Crabtree and Bridgewater (23) have proposed a similar classification system. However, they do not agree with the Reynolds number ranges proposed by Narayanan, et al. Collins (21) has described the behavior of wakes of two-dimensional bubbles from Classes IV and V when bubble breakup occurs. Lindt (47) has determined that the ratio of the translational vortex velocity to the bubble rise velocity for Class IV bubbles is 0.2. This value was determined using two-dimensional bubbles.

Narayanan, et al. (51) have also measured the vortex length of bubbles in Class III. This was done photographically by observing cine films to determine the distance at which a trailing bubble acquired an unsteady velocity. These experiments were carried out in aqueous solutions of glycerin having viscosities in the range of 0.9 to 9.0 poise at 21°C. Narayanan, et al. correlate the ratio of the vortex length to bubble basel diameter as a function of bubble Reynolds number. Guthrie and Bradshaw (33) have also measured wake lengths for gas bubbles in aqueous PVA solutions. Yeleskel and Kebat (199) have measured wake-to-drop volume ratios of drops in seven different liquid/liquid systems. Drop Reynolds numbers in these experiments ranged from 137 to 798.

Bubble Coalescence.--Bubble coalescence in gas/liquid flow is extremely complex, It can be dominated by surface phenomena or by the fluid mechanics of the system. The latter includes wake and liquid circulation effects.

Koide, et al. (42) have pointed out the importance of surfactants on bubble coalescence. They found that the addition of a surfactant such as Tween 20 or isoamylalcohol, or an inorganic salt to water could significantly reduce the bubble size produced by a gas distributor at a given flow rate. In addition, Anderson and Quinn (12) and other investigators (185,195) have found evidence that there are surface active contaminates which can promote coalescence.

As stated above, wake effects can play an important role in bubble coalescence. Attempts to quantify the effect are based on experiments involving two vertically aligned bubbles. Crabtree and Bridgwater (22) have studied this problem in aqueous sucrose solutions. In these experiments the bubble Reynolds numbers were in the range of 40 to 90 and bubble volumes ranged from 10 to 44 cc. They propose that the rise velocity of the lower bubble has an additional component due to the wake of the top bubble. Using a viscous model to describe the wake velocity, they developed a model to predict coalescence times and distances. Bubbles with volumes as large as 40 cc were found to coalesce at initial separation distances of up to 70 cm. The authors correlate their data by expressing the apparent wake velocity as a function of the separation distance. These quantities are made dimensionless with respect to the velocity and radius of the leading bubble, respectively.

Narayanan, et al. (51) have performed similar experiments. In their experiments the bubble Reynolds numbers ranged from 0.5 to 80 (Class I through III). Equations were developed relating the relative velocities of the two bubbles.

In bubble swarms of equal size, free from contaminate effects, the mechanism of coalescence becomes one of bubble clustering and the subsequent thinning of the film separating the bubbles. Lockett and Kirkpatrick (48), Hills (36), Anderson and Quinn (12), and Calderbank, et al. (17) have all indicated the importance of the liquid circulation pattern in bubble clustering.

Calderbank, et al. have studied CO_2 bubble clustering in aqueous solutions of glycerol with viscosities ranging from 1 to 100 centipoise. They describe the clustering of small ellipsoidal bubbles at the bottom of their column. Excellent pictures are presented of the process. It was found that liquid viscosity determines the extent of coalescence; above 70 cp the rate of coalescence was extremely rapid. It was also observed that the clusters were formed in the center of the column, thus indicating the bubbles have a radial velocity due to liquid circulation. Calderbank, et al. also developed the following model to predict the rate of bubble cluster formation:

$$\frac{f}{A} = \frac{6U_t}{d^3_{sm}\beta}\left(\frac{6}{4}\pi\right)^{2/3\ 1/3}\epsilon_g^{\beta-1}\ ^{(2\beta+1)/3} \qquad (16)$$

where: f = frequency of formation of clusters
d_{sm} = Sauter-mean bubble diameter
A = cross-sectional area of column
β = number of small bubbles forming the cluster

Once the cluster formed, Calderbank, et al. observed the thinning of the film between the bubbles and the formation of a spherical cap bubble. Kirkpatrick and Lockett (40) have modelled the thinning of the film between two equal-sized bubbles approaching each other. These authors developed expressions for the distance from the coalescing bubbles' centers to the adjoining film and the thickness of the film as functions of time. When these expressions were simultaneously solved, it was found that increasing the approach velocity or the bubble diameter increased the time for film rupture (coalescence). Kirkpatrick and Lockett measured the contact times for bubbles in clouds and found them to be small compared to the times calculated for coalescence to occur.

Hills (35) has shown that once a spherical cap bubble has formed, smaller bubbles never collide with its nose. If smaller bubbles are to coalesce with larger bubbles, they must first become trapped in the wake of the larger bubble. Calderbank, et al. have also made similar observations.

Bubble Breakup.--Once a large bubble is formed, the question of its stability arises. Clift and Grace (19) propose that gas bubbles in fluids break up via a Taylor instability. Taylor (59) has shown that for inviscid fluids, small disturbances on a horizontal surface between the fluids grow if the upper fluid is more dense than the lower fluid. The rate of growth of the disturbance is proportional to

$$\sqrt{\frac{-g(\rho_2-\rho_1)}{(\rho_2+\rho_1)}}$$

where ρ_1 and ρ_2 are the density of the upper and lower fluids, respectively. Bellman and Pennington (15) have extended the analysis of Taylor to include the effects of surface tension and viscosity. They found when the effect of surface tension was included in the analysis that only disturbances with wavelengths greater than that given by the following relation would grow:

$$\lambda > 2\pi\left(\frac{\sigma}{-g(\rho_2-\rho_1)}\right)^{1/2} \qquad (17)$$

The wavelength which grows the fastest is given by:

$$\lambda = 2\pi \left(\frac{3\sigma}{-g(\gamma_2 - \gamma_1)} \right)^{1/2} \tag{18}$$

When the effect of viscosity is also included in the analysis, the range of wavelengths which grow (given by Equation 17) does not change. However, the wavelength which grows the fastest does change in a rather complex manner. In general, increasing the viscosity increases the wavelength of the fastest growing disturbance..

Swarms of Bubbles.--An important consideration in modelling vertical bubble flow is the effect of neighboring bubbles on the rising velocity of a bubble. In the ideal bubbly regime the effect is usually considered to be only a bubble concentration effect. However, for the churn-turbulent flow pattern, the interaction is more complex as the bubbles can influence the global liquid flow pattern.

Numerous models have been proposed for the ideal bubbly regime. In general these models relate the slip velocity of the bubble swarm to the terminal velocity of a single bubble and the gas holdup. The slip velocity is defined as:

$$U_s = \frac{U_g}{\epsilon_g} - \frac{U_l}{1-\epsilon_g} \tag{19}$$

Lockett and Kirkpatrick (48) have reviewed the various models. They are:

1) $U_s = U_t$ proposed by Turner (60).

2) $U_s = U_t/(1-\epsilon_g)$ proposed by Davidson and Harrison (24).

3) $U_s = U_t(1-\epsilon_g)^{n-1}$--a Richardson and Zaki type relationship proposed by Bridge, et al. (16).

4) $U_s = U_t(1-\epsilon_g)/(1-\epsilon_g^{5/3})$ proposed by Marrucci (49).

Wallis (61) has also proposed a Richardson-Zaki type model. Following Wallis (61), it is convenient to define the gas drift flux as:

$$V_{CD} = \epsilon_g(1-\epsilon_g)U_S \tag{20}$$

Physically the gas drift flux is the volumetric flux of gas relative to a surface moving at the average velocity (gas plus liquid). The above models rewritten in terms of the drift flux are:

1) Turner: $V_{CD} = U_t\epsilon_g(1-\epsilon_g)$ (21)

2) Davidson and Harrison: $V_{CD} = U_t\epsilon_g$ (22)

3) Richardson and Zaki: $V_{CD} = U_t\epsilon_g(1-\epsilon_g)^n$ (23)

4) Marrucci: $V_{CD} = U_t\epsilon_g(1-\epsilon_g)^2/1-\epsilon_g^{5/3}$ (24)

Lockett and Kirkpatrick measured V_{CD} as a function of ϵ_g up to $\epsilon_g = 0.66$ for 5 mm diameter bubbles. They found the Richardson-Zaki model with n = 2.39 gave the best correlation. However, at ϵ_g greater than approximately 0.25, even this correlation had to be multiplied by an empirical correction factor given by:

$$f(\epsilon_g) = 1 + 2.55\epsilon_g^3 \tag{25}$$

They suggest that this correction factor arises because of bubble deformation at high ϵ_g. Davidson and Harrison (24) also analyzed the air/water data of Bridge, et al. (16) and found them correlated best via a Richardson-Zaki type model with n = 2.39. The highest gas holdup for these data was 0.20, and the bubble size was 3.5 mm. The data of Nicklin (53) have also been analyzed in terms of the drift flux approach. Nicklin does not state the size of his bubbles. However, extrapolation of his data to $U_g = 0$ indicates U_t for his bubbles is 240 mm/sec. These results are presented in Figure 9, along with sketches of the various models with U_t = 240 mm/sec. For reference, a line representing typical data (Wallis, Ref. 61) in the churn-turbulent regime is included in Figure 9.

Also sketched in Figure 9 are several dashed lines representing typical transition data between the ideal bubbly and churn-turbulent regimes (Wallis, Ref. 61). This transition can occur at any value of ϵ_g. Lockett and Kirkpatrick (48) have discussed the bubble coalescence mechanisms by which the transition occurs. These include liquid circulation and the formation of large bubbles. The latter can be formed by distributor plate effects or by bubble clustering further up the column. Both liquid circulation and large bubble effects lead to a non-uniform radial distribution of gas.

Hills (36) has measured the radial distribution of gas holdup with a conductivity probe in a 138 mm column. In the churn-turbulent regime he found the holdup at the center line can be four times that at the wall. Using a modified Pitot tube, he also measured the radial